

A Unified Deep Reinforcement Learning Approach for Close Enough Traveling Salesman Problem

Mingfeng Fan*, Jiaqi Cheng*, Yaxin Wu, Yifeng Zhang[†], Yibin Yang, Guohua Wu, and Guillaume Sartoretti

Abstract—In recent years, deep reinforcement learning (DRL) has gained traction for solving the NP-hard traveling salesman problem (TSP). However, limited attention has been given to the close-enough TSP (CETSP), primarily due to the challenge introduced by its neighborhood-based visitation criterion, wherein a node is considered visited if the agent enters a compact neighborhood around it. In this work, we formulate a Markov decision process (MDP) for CETSP using a discretization scheme and propose a novel unified dual-decoder DRL (UD3RL) framework that separates decision-making into node selection and waypoint determination. Specifically, an adapted encoder is employed for effective feature extraction, followed by a node-decoder and a loc-decoder to handle the two sub-tasks, respectively. A k -nearest neighbors subgraph interaction strategy is further introduced to enhance spatial reasoning during location decoding. Furthermore, we customize the REINFORCE algorithm to train UD3RL as a unified model capable of generalizing across different problem sizes and varying neighborhood radius types (i.e., constant and random radii). Experimental results show that UD3RL outperforms conventional methods in both solution quality and runtime, while exhibiting strong generalization across problem scales, spatial distributions, and radius ranges, as well as robustness to dynamic environments.

Index Terms—Close-enough TSP, deep reinforcement learning, dual-decoder.

I. INTRODUCTION

THE close-enough traveling salesman problem (CETSP) is a well-known variant of the classical traveling salesman problem (TSP) that preserves its NP-hard complexity [1]. CETSP poses a hybrid optimization challenge, combining the discrete task of determining the visiting sequence, as in the standard TSP, with the continuous optimization of selecting specific visiting locations within designated neighborhoods [2]. Unlike the traditional TSP, where the agent must visit each target node directly, CETSP requires only that the agent passes through any point within a predefined neighborhood of each target, typically modeled as a circular region centered around the node, as shown in Fig. 1. This

Mingfeng Fan and Jiaqi Cheng contributed equally to this work.

Mingfeng Fan, Yifeng Zhang, and Guillaume Sartoretti are with the Department of Mechanical Engineering, National University of Singapore, Singapore (E-mail: ming.fan@nus.edu.sg, yifeng@u.nus.edu, guillaume.sartoretti@nus.edu.sg).

Jiaqi Cheng is with the School of Traffic and Transportation Engineering, Central South University, China (E-mails: chengjq@csu.edu.cn).

Yaxin Wu is with the Department of Industrial Engineering and Innovation Sciences, Eindhoven University of Technology, Netherlands. (E-mail: wyxacc@hotmail.com)

Yibin Yang is with the School of Vehicle and Mobility, Tsinghua University, China. (E-mail: yangyb15@gmail.com)

Guohua Wu is with the School of Automation, Central South University, China. (E-mail: guohuawu@csu.edu.cn)

Corresponding authors: Yifeng Zhang.

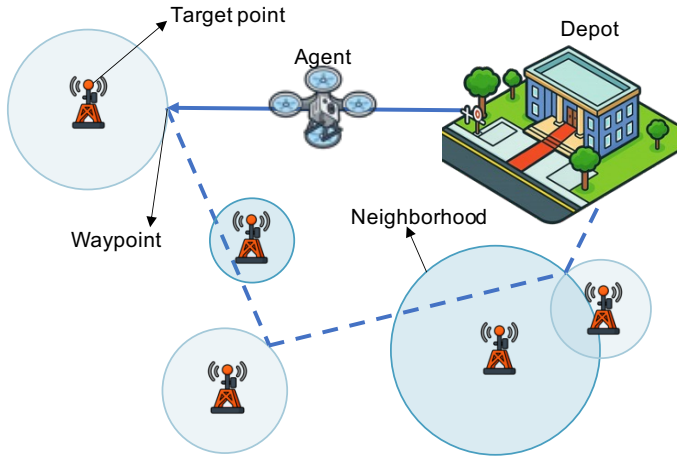


Fig. 1: An example path in the CETSP, where an agent is required to visit a set of target neighborhoods, each represented by a circular region.

relaxed visiting requirement makes CETSP highly applicable to various real-world scenarios, such as drone-based RFID tag reading [3], robotic inspection of wireless sensor networks [4], and solar panel diagnostic reconnaissance [5], among others.

Many approaches have been proposed in the literature to solve the CETSP, which can generally be categorized into exact and heuristic algorithms. Exact algorithms [6], [7] are capable of providing optimal solutions for moderately sized instances, but they suffer from scalability issues and are impractical for large-scale problems. Heuristic methods [2], [8], while able to handle larger instances, tend to become computationally expensive as the problem size increases, and often rely heavily on domain-specific knowledge, limiting their adaptability. In recent years, deep reinforcement learning (DRL) has emerged as a promising alternative, attracting considerable attention for addressing combinatorial optimization problems (COPs), with notable examples including AM [9] and POMO [10]. Compared to traditional methods, DRL offers lower inference costs and greater flexibility across different problem domains.

Despite their success, DRL-based methods have rarely been applied to the CETSP, primarily due to the additional complexity of determining specific visiting locations within each neighborhood after establishing the node visiting sequence. This subtask can be formulated as a second-order cone programming (SOCP) problem, and its outcome may in turn influence the optimal visiting sequence, creating a bidirectional dependency that is challenging for existing DRL frameworks

to handle effectively.

To overcome this challenge, we first apply a discretization scheme to convert the continuous neighborhoods of nodes into a finite set of candidate waypoints. We then propose a unified dual-decoder DRL framework, termed UD3RL, which solves the resulting discretized CETSP by decoupling the decision-making process into node selection and waypoint selection. Specifically, UD3RL employs an adapted Transformer encoder to extract meaningful problem representations and utilizes a node-decoder and a loc-decoder to sequentially select the next node to visit and the precise location (i.e., waypoint) within its neighborhood. Unlike previous methods that only determine waypoints after the complete node sequence is fixed, the architecture of UD3RL is naturally suited to both static and dynamic environments. Our contributions are summarized as follows.

- 1) We propose a flexible architecture, UD3RL, for solving both static and dynamic CETSP instances. It features a node-decoder for selecting the next node to visit and a loc-decoder for determining the waypoint to visit within the neighborhood of the chosen node.
- 2) We introduce a k -nearest neighbors (k -NN) subgraph interaction strategy to guide the DRL agent toward optimal waypoint selection during the loc-decoder process.
- 3) We customize the REINFORCE algorithm to train UD3RL as a unified model capable of generalizing across different problem sizes and varying neighborhood radius types (i.e., constant and random radii).
- 4) We conduct extensive experiments to validate the effectiveness of UD3RL. Results demonstrate that UD3RL outperforms relevant conventional and hybrid approaches in both solution quality and generalization capability.

The remainder of this paper is organized as follows: Section II reviews traditional methods for solving the CETSP and DRL approaches for TSP. Section III presents the problem definition and Markov Decision Process (MDP) model for CETSP. Section IV details the proposed UD3RL framework. Section V reports and analyzes the experimental results. Finally, Section VI concludes the paper and discusses potential directions for future work.

II. RELATED WORKS

In this section, we review conventional methods for solving the CETSP as well as DRL approaches for the TSP. To the best of our knowledge, this is the first work to employ DRL for solving the CETSP.

A. Conventional Methods for CETSP

The CETSP was first addressed in [3], which proposed a three-phase heuristic consisting of: (1) selecting a feasible set of supernodes \mathcal{G} , (2) generating a feasible tour τ over the points in \mathcal{G} , and (3) improving the tour τ . Following this framework, subsequent works [8], [11], [12] adopted similar three-step heuristics based on the concept of Steiner zones. Exact algorithms include mixed-integer programming (MIP) approaches based on discretization schemes [1], [6], [13] and

a branch-and-bound algorithm utilizing SOCP [7]. While MIP-based methods offer flexible modeling, their solution quality heavily depends on the discretization granularity. The SOCP-based approach can yield optimal solutions for moderately sized instances but does not scale well to larger problems. Building on [13], Carrabs et al. [14] proposed a meta-heuristic method incorporating an adaptive discretization scheme. Other heuristic methods [2], [5] directly tackle CETSP using meta-heuristics combined with SOCP formulations. However, such heuristics often require substantial expert knowledge and become computationally expensive as problem size increases, limiting their practical scalability.

B. DRL Approaches for TSP

DRL models can learn effective patterns from large datasets without relying on handcrafted heuristics or domain-specific knowledge, enabling strong generalization to unseen instances [15]. Moreover, once trained, DRL models offer high inference efficiency. These advantages have led to a surge of research applying DRL to solve the classical TSP in recent years. Based on their solution generation strategies, DRL-based routing methods can be broadly classified into two categories: *improvement-based* approaches [16]–[21] and *construction-based* approaches [9], [10], [22]–[25]. Among these, construction-based methods generally exhibit faster inference times [26], [27], making them particularly suitable for solving the CETSP. Specifically, Bello et al. [22] proposed one of the earliest DRL-based methods for the TSP by training a pointer network (PtrNet) [28] using an actor-critic framework. Subsequently, Kool et al. [9] introduced the attention model (AM), which replaced PtrNet with a Transformer-based architecture [29] to achieve higher solution quality. Building on this, POMO [10] further improved performance by leveraging multiple parallel solution trajectories and applying data augmentation to address the symmetry in routing problems, achieving near-optimal results for the TSP. More recent works [30], [31] integrate supervised learning to further improve performance. However, due to the complexity of CETSP, these DRL-based methods are not directly applicable for solving CETSP.

III. PRELIMINARIES

A. Problem Definition and Notation

Let there be $n+1$ nodes located in a two-dimensional plane, indexed by the set $N = \{0, 1, \dots, n\}$, and let index 0 denote the depot and indexes in $\{1, 2, \dots, n\}$ as the *target points*. Each node $i \in N$ is associated with a closed disk C_i centered at $o_i = \{cx_i, cy_i\}$ with radius r_i where $r_0 = 0$. We define the *neighborhood* of node i as $\mathcal{N}(i) := C_i$ where $C_0 = o_0$. The objective of the CETSP is to find the shortest tour τ^* that starts and ends at the depot 0 and intersects the neighborhood $\mathcal{N}(i)$ for every target point, in any order. Let $\{y_0, y_1, y_2, \dots, y_g\}$ where $y_0 = o_0$ be the set of *waypoints* in the tour τ , i.e., points at which the tour changes direction. Any tour τ can be uniquely identified by its sequence of waypoints. The cost of an edge $y_i y_{i+1}$ is defined as the Euclidean distance between y_i and y_{i+1} . The total cost of a tour τ is denoted as $L(\tau)$, which

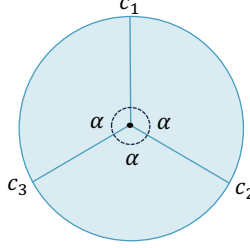


Fig. 2: PDS for $\gamma = 3$ with $\hat{\mathcal{N}}(i) = \{c1, c2, c3\}$ and $\alpha = 120^\circ$.

is the sum of the edge lengths: $L(\tau) = \sum_{i=0}^{g-1} \|y_{i+1} - y_i\| + \|y_0 - y_g\|$. The goal is to find an optimal tour τ^* such that $\tau^* = \arg \min_{\tau} L(\tau)$ subject to the constraints that τ forms a cycle starting and ending at the depot o_0 , and intersects all neighborhoods $\mathcal{N}(i)$ for all target points.

B. Discretization Scheme

Since each neighborhood $\mathcal{N}(i)$, $i \in \{1, \dots, n\}$, contains an infinite number of possible waypoints, the number of feasible tours for the CETSP is also infinite. However, any specific feasible tour consists of only a finite number of waypoints. Therefore, it is possible to associate each feasible solution with a discrete set of points. Specifically, we discretize each neighborhood $\mathcal{N}(i)$ using a fixed number γ of points, denoted by $\hat{\mathcal{N}}(i) = \{c_1, \dots, c_\gamma\}$. Let $\hat{\tau}$ represent a feasible CETSP tour constructed by selecting one point from each neighborhood in a subset of the node set N . Note that it is not necessary to select a discretization point from every neighborhood, as some edges in $\hat{\tau}$ may pass through certain neighborhoods without explicitly visiting a discretized point within them. The cost of any such tour $\hat{\tau}$ can be computed based on the Euclidean distances between the selected points. The shortest tour $\hat{\tau}^* = \arg \min_{\hat{\tau}} L(\hat{\tau})$.

We adopt the *Perimetral Discretization Scheme* (PDS) [1], motivated by the observation that the waypoints of the optimal tour τ^* are always located on the boundaries of the neighborhoods [6]. PDS places discretization points uniformly along the circumference of each target neighborhood. Specifically, let γ denote the number of points used to discretize each neighborhood $\mathcal{N}(i)$. Then, the PDS divides the circumference C_i of each neighborhood into γ equal circular arcs with central angle $\alpha = \frac{360^\circ}{\gamma}$, and places discretization points at the endpoints of these arcs, as shown in Fig. 2. For the classical TSP with n cities, the time complexity is $\mathcal{O}(n!)$. In contrast, after applying PDS to the CETSP, the solution space expands to all sequences of discretization points, resulting in a time complexity of $\mathcal{O}(n! \gamma^n)$, which is significantly higher than that of the TSP due to the added combinatorial burden from continuous-to-discrete transformation.

C. MDP for CETSP

The route construction in CETSP after PDS can be viewed as a sequential decision-making process, which can be naturally modeled as an MDP and solved using reinforcement learning (RL). We define the elements of the MDP, including

the state space, action space, transition rule, and reward function, as follows.

State: The state at time step t , denoted by $S_t = \{\pi_t, Z_t\}$, consists of the current partial solution π_t and the set of already visited target points Z_t .

The partial solution $\pi_t = \{X_t, \hat{\tau}_t\}$ includes:

- The sequence of selected nodes up to time step t , denoted by $X_t = \{x_0, x_1, \dots, x_t\}$, where x_0 is the depot and $x_j \in N$.
- The corresponding sequence of selected discretization points (i.e., waypoints) $\hat{\tau}_t = \{y_0, y_1, \dots, y_t\}$, where $y_j \in \hat{\mathcal{N}}(x_j)$ for $j > 0$, and $y_0 = o_0$ is the depot coordinate.

The visited set $Z_t = \bigcup_{j=1}^t z_j$, where each $z_j \subseteq N$ contains the set of target points whose neighborhoods are intersected by the edge $y_{j-1}y_j$ at time step j .

Action: At each time step t , the agent selects an action $a_t = (x_{t+1}, y_{t+1})$, where $x_{t+1} \in N \setminus Z_t$ is the next node to be visited, and $y_{t+1} \in \hat{\mathcal{N}}(x_{t+1})$ is a discretization points within its neighborhood. The process continues until the terminal state is reached, i.e., when the agent returns to the depot and completes the tour.

Transition: The next state $S_{t+1} = (\pi_{t+1}, Z_{t+1})$ is determined by the selected action $a_t = (x_{t+1}, y_{t+1})$ at time step t . The partial solution is updated by appending the new node and waypoint to the current state, i.e., $\pi_{t+1} = (X_{t+1}, \hat{\tau}_{t+1}) = (X_t \cup \{x_{t+1}\}, \hat{\tau}_t \cup \{y_{t+1}\})$. If $x_{t+1} = 0$ (i.e., the depot), then $y_{t+1} = o_0$, and the process transitions to the terminal state. The set of visited nodes is updated by merging Z_t with the set of newly passed nodes z_{t+1} , whose neighborhoods are intersected by the edge y_ty_{t+1} , i.e., $Z_{t+1} = Z_t \cup z_{t+1}$.

Reward: To encourage shorter tours, the reward is defined as the negative of the total travel distance. The cumulative reward for a complete tour $\hat{\tau} = \{y_0, y_1, \dots, y_T\}$ is given by: $R = -L(\hat{\tau})$, where $L(\hat{\tau})$ is the total Euclidean length of the tour constructed from the sequence of selected waypoints.

IV. METHODOLOGY

In this section, we introduce the proposed UD3RL (unified dual-decoder DRL), including its architecture and training algorithm.

A. Overview

As illustrated in Fig. 3, the UD3RL policy network p_θ with trainable parameters θ is tailored to address the CETSP and consists of an adapted Transformer encoder, a node-decoder, and a loc-decoder. The encoder processes the input node features, which include the depot location, target locations, and the radii of their respective neighborhoods, and maps them into feature embeddings, thereby extracting essential information from the data. Given the feature embeddings and problem-specific constraints, the node-decoder selects the next node to visit. Subsequently, the loc-decoder determines the exact waypoint within the chosen node's neighborhood. The two decoders sequentially select actions at each time step to construct a complete solution.

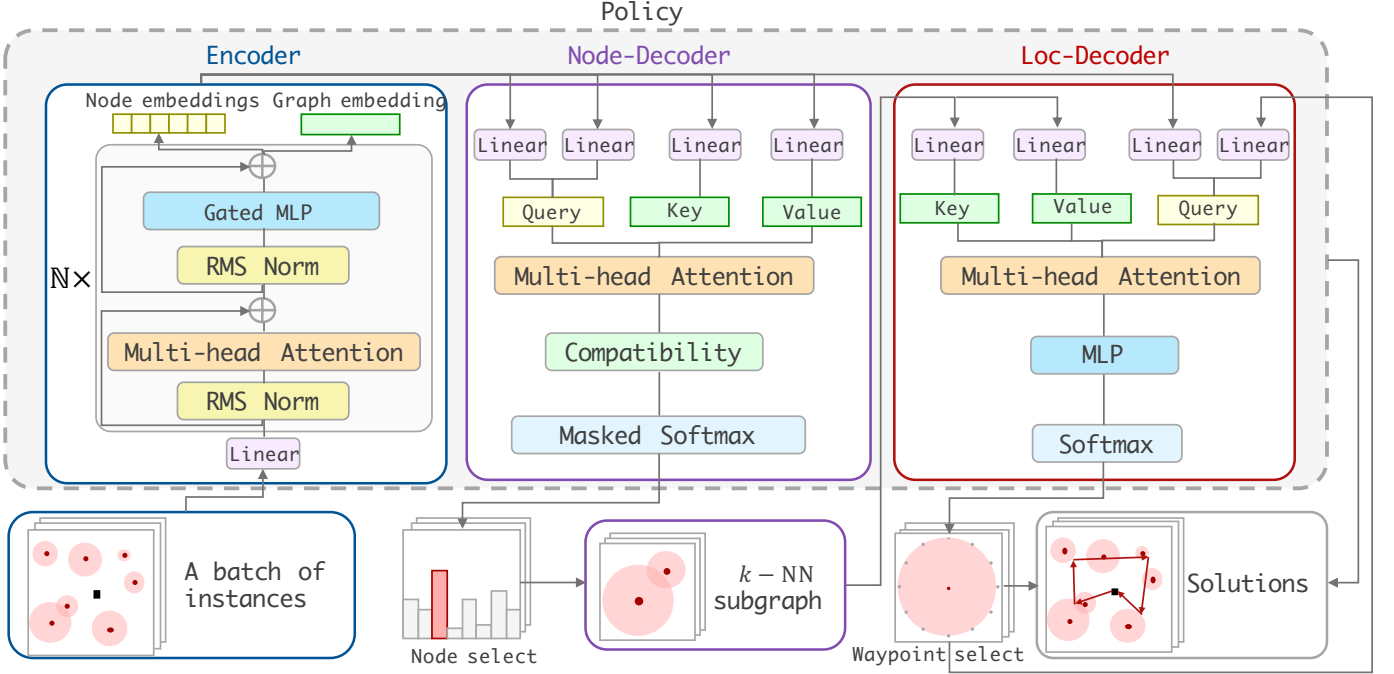


Fig. 3: Architecture of the policy network used in our method. It consists of an adapted Transformer encoder, a node-decoder, and a loc-decoder. Given a batch of instances, the encoder generates node embeddings and a graph embedding. Based on these, the node-decoder outputs selection probabilities for the next node to visit, while the loc-decoder computes probabilities over candidate waypoints within the selected neighborhood. The loc-decoder also incorporates k -NN subgraph information to enhance spatial decision-making.

The final output of the policy network p_θ is a sequence of action tuples (x_t, y_t) , consisting of selected nodes and their corresponding waypoints. The output solution is denoted as $\pi = \{(x_0, y_0), (x_1, y_1), \dots, (x_T, y_T)\}, x_t \in N, y_t \in \hat{\mathcal{N}}(x_t)$, where T is the time step limits for solution construction. The probability of generating a solution π is defined by the learned policy p_θ as:

$$P(\pi | \lambda) = \prod_{t=1}^T p_\theta((x_t, y_t) | \lambda, (x_{0:t-1}, y_{0:t-1})), \quad (1)$$

where λ represents the current CETSP instance, and the policy is conditioned on the problem input and the partial solution up to time t .

B. Transformer Encoder

The encoder is an adaptation of the AM [9], consisting of a stack of attention layers. Each layer includes a multi-head attention (MHA) sublayer and a feed-forward (FF) sublayer, enhanced by several key modifications. Building on [32], we replace the original ReLU-activated MLP with a SiLU-activated gated MLP [33] in the FF sublayer, further enhancing representational power. Additionally, we apply root mean square (RMS) normalization [34] in place of layer normalization and adopt a pre-norm structure (i.e., applying normalization before the residual connections) in each sublayer to improve training stability and accelerate convergence.

Raw Features to Hidden States. We use the node coordinates $\{o_i\}_{i=0}^n$ and their corresponding neighborhood radii $\{r_i\}_{i=0}^n$

as raw input features. We project the target point coordinates and neighborhood radii into their respective embeddings using linear transformations:

$$h_{o,0}^i = W_o o_i, \quad h_{r,0}^i = W_r r_i, \quad \forall i \in N, \quad (2)$$

where W_o and W_r are learnable projection matrices. The initial node embeddings are then formed by concatenating the coordinate and radius embeddings: $h_0^i = [h_{o,0}^i; h_{r,0}^i], \forall i \in N$. These node embeddings $h_0 = \{h_0^i\}_{i=0}^n$ are subsequently passed through N stacked attention layers to refine and enrich their representations.

MHA Sublayer. The MHA sublayer captures dependencies between different nodes in the input sequence. Given the node embeddings $h_{l-1} = \{h_{l-1}^i\}_{i=0}^n$ as inputs to the l -th attention layer, we first employ RMS normalization to obtain pre-norm node embeddings:

$$h_{l-1}' = \text{RSMNorm}(h_{l-1}). \quad (3)$$

We begin by linearly projecting the pre-normalized node embeddings h_{l-1}' into *queries* Q , *keys* K , and *values* V , using H distinct subspaces (attention heads). Each projection is performed using learned weight matrices W_j^Q , W_j^K , and W_j^V , such that for each head $j = 1, \dots, H$:

$$Q_j = h_{l-1}' W_j^Q, \quad K_j = h_{l-1}' W_j^K, \quad V_j = h_{l-1}' W_j^V.$$

The attention weights for each head are computed using scaled dot-product attention, followed by a softmax operation:

$$A_j = \text{Softmax} \left(\frac{Q_j K_j^\top}{\sqrt{d_k}} + M \right), \quad (4)$$

where d_k is the dimensionality of the key vectors, used as a scaling factor to stabilize gradients, and M is an optional attention mask. This mask can be used to prevent attending to infeasible actions by setting corresponding entries to $-\infty$. Note that the attention mask is not applied during the encoder. The output of each attention head is then computed as the weighted sum of the projected values:

$$Z_j = A_j V_j.$$

The outputs from all heads are concatenated and passed through a final linear projection using a learned matrix W^O , producing the final output of the multi-head attention (MHA) module:

$$\text{MHA}(Q, K, V) = \text{Concat}(Z_1, \dots, Z_H) W^O. \quad (5)$$

Finally, the output of the MHA sublayer is obtained by applying a residual connection that adds the original input h_{l-1} to the MHA output:

$$\hat{h}_{l-1} = h_{l-1} + \text{MHA}(Q, K, V). \quad (6)$$

FF Sublayer. The embeddings \hat{h}_{l-1} from the MHA sublayer are passed into the feed-forward (FF) sublayer, which consists of RMS normalization, a SiLU-activated gated MLP [33], and a residual connection. The computations are defined as follows:

$$\hat{h}'_{l-1} = \text{RMSNorm}(\hat{h}_{l-1}), \quad (7)$$

$$h^f_{l-1} = \left(\hat{h}'_{l-1} \odot \sigma(W_1 \hat{h}'_{l-1} + b_1) \right) \otimes \text{SiLU} \left(W_2 \hat{h}'_{l-1} + b_2 \right), \quad (8)$$

$$h_l = \hat{h}_{l-1} + h^f_{l-1}, \quad (9)$$

where \odot denotes element-wise multiplication, \otimes denotes matrix multiplication, σ is the sigmoid activation function, SiLU is the Sigmoid Linear Unit (also known as Swish), and W_1, W_2, b_1, b_2 are learnable parameters.

We stack \mathbb{N} attention layers (with $\mathbb{N} = 6$ in our implementation) in the encoder, each following the same architecture but with independent parameters. The final node embeddings $h_{\mathbb{N}}$ produced by the encoder serve as inputs to both the node-decoder and the loc-decoder.

C. Dual-decoder

The dual-decoder architecture consists of two components: the *node-decoder*, which selects the next node to visit (including both target points and the depot), and the *loc-decoder*, which determines the precise waypoint within the corresponding neighborhood that the agent should pass through. At each time step, the node-decoder and loc-decoder operate sequentially. Moreover, the output of the node-decoder serves as part of the input to the loc-decoder. To enhance the loc-decoder's contextual awareness, we incorporate k -NN graph information. This augmentation enables the policy network

to better capture the local spatial structure, allowing the loc-decoder to make more precise decisions regarding traversal waypoints. We elaborate on the designs of the node-decoder and loc-decoder in the following subsections.

Node-decoder. The node-decoder generates a probability distribution for selecting the next node to visit, leveraging two primary embeddings: the node embeddings $h_{\mathbb{N}}$ produced by the encoder, and the context embedding q_t^c . The context embedding q_t^c is constructed by combining the graph embedding $\bar{h}_{\mathbb{N}} = \frac{\sum_{i=0}^n h_{\mathbb{N}}^i}{n+1}$ with the embedding $h_{\mathbb{N}}^{x_t}$ of the last visited node x_t , as follows,

$$Q_t^c = \bar{h}_{\mathbb{N}} W_Q^g + h_{\mathbb{N}}^{x_t} W_Q^l, \quad (10)$$

where W_Q^g and W_Q^l are trainable matrices. Similar to [9], the node-decoder comprises an MHA layer and a compatibility layer. We regard the context embedding Q_t^c as a query to attend to all nodes. To this end, we derive the keys and values from node embeddings $h_{\mathbb{N}}$ such that,

$$K^c = h_{\mathbb{N}} W_K^c; \quad V^c = h_{\mathbb{N}} W_V^c, \quad (11)$$

where W_K^c and W_V^c are trainable parameters. Then the query Q_t^c , keys K^c , and values V^c are input to the MHA layer to produce an updated context vector h_t^c as follows,

$$h_t^c = \text{MHA}(Q_t^c, K^c, V^c, M_t), \quad (12)$$

where M_t is the attention mask applied at time step t , used to assign $-\infty$ to the attention scores of infeasible nodes. These infeasible nodes are those whose neighborhoods have already been visited in the agent's current partial tour. This updated context vector h_t^c is subsequently processed through the compatibility layer, along with $h_{\mathbb{N}}$, to compute the final probability distribution over all nodes via a masked softmax layer as follows,

$$p_{\text{node}} = \text{Softmax} \left(C \cdot \text{Tanh} \left(\frac{h_{\mathbb{N}} h_t^c}{\sqrt{d_k}} \right) + M_t \right). \quad (13)$$

To enhance solution diversity, we adopt the *multistart* strategy from POMO [10], which generates n parallel trajectories simultaneously. All trajectories begin with the depot as the first node-action, since the agent must start from the depot. For the second node-action, we explicitly assign each trajectory a unique target point from the set $\{1, 2, \dots, n\}$, ensuring diverse starting paths. For subsequent time steps, node-actions are selected according to the learned probability distribution p_{node} .

Loc-Decoder. Given the node embeddings $h_{\mathbb{N}}$ from the encoder and the selected node x_{t+1} from the node-decoder, the loc-decoder, comprising an MHA layer, a MLP, and a softmax layer, determines the precise waypoint within the neighborhood of the selected node. Using PDS [1], the neighborhood (i.e., a circular region) is discretized into γ points evenly spaced along its circumference. A probability distribution p_{loc} over these candidate waypoints is generated similarly to the node-decoder.

In the MHA layer, the query Q_t^l is computed via a linear transformation of the embedding $h_{\mathbb{N}}^{x_{t+1}}$ of the selected node x_{t+1} , and the previous location y_t , as follows:

$$Q_t^l = h_{\mathbb{N}}^{x_{t+1}} W_Q^n + y_t W_Q^y, \quad (14)$$

where W_Q^n and W_Q^y are learnable projection matrices. Meanwhile, the keys and values are constructed from a k -NN subgraph centered at the selected node x_{t+1} , defined as:

$$\tilde{N}_k(x_{t+1}) = \left\{ h_{\mathbb{N}}^{x^{(1)}}, h_{\mathbb{N}}^{x^{(2)}}, \dots, h_{\mathbb{N}}^{x^{(k)}} \right\},$$

where $\{x^{(1)}, \dots, x^{(k)}\}$ are the k nearest neighbors of x_{t+1} determined by Euclidean distance. The keys and values are then computed as:

$$K_t^l = \tilde{N}_k(x_{t+1})W_K^l, \quad V_t^l = \tilde{N}_k(x_{t+1})W_V^l, \quad (15)$$

where W_K^l and W_V^l are learnable matrices. The output of the MHA layer is then given by:

$$h_t^l = \text{MHA}(Q_t^l, K_t^l, V_t^l). \quad (16)$$

This interaction between the current route direction (from the previous location y_t to the selected node x_{t+1}) and the local subgraph context allows the policy network to more effectively identify optimal traversal points within the neighborhood.

The resulting representation h_t^l is passed through a three-layer MLP, followed by a softmax layer to produce the probability distribution over the γ candidate waypoints:

$$p_{\text{loc}} = \text{Softmax}(W_f^3 \cdot g(W_f^2 \cdot g(W_f^1 h_t^l))), \quad (17)$$

where W_f^1, W_f^2, W_f^3 are learnable weight matrices, and $g(\cdot)$ is the activation function. The loc-decoder then selects the waypoint y_{t+1} based on the probability distribution p_{loc} , in a manner analogous to the node-decoder.

During training, the dual-decoder selects actions (i.e., node-waypoint pairs) using a sampling strategy, drawing actions according to their probabilities to promote exploration in the solution space. During testing, a greedy strategy is used, selecting the most probable action at each step to construct the final solution. This trade-off ensures efficient exploration during training and fast inference during deployment.

D. Objective and Optimization

The customized REINFORCE algorithm for UD3RL is summarized in Algorithm 1, where we adopt the policy gradient with a shared baseline to train the policy of node selection and waypoint determination for solution construction. Given an instance s , we generate multiple solutions in which the second nodes are forced to select different target points. Besides, the policy network π_θ picks an action tuple $a_t = \{x_{t+1}, y_{t+1}\}$ at each time step and generates probability vectors for both nodes and waypoints (i.e., the discrete points along the circumference of the circle) corresponding to the chosen node. Then, we calculate the rewards of these solutions as the negative of the total travel distances. With the rewards, we customize REINFORCE [35] to compute the gradient for maximizing the expected return $J(\theta) = E_{\pi \sim p_\theta, s \sim \mathcal{S}_I, \lambda \sim \mathcal{S}_\lambda, \kappa \sim \Lambda} R(\pi|s, \lambda, \kappa)$ such that,

$$\begin{aligned} \nabla J(\theta) = & E_{\pi \sim p_\theta, s \sim \mathcal{S}_I, \lambda \sim \mathcal{S}_\lambda, \kappa \sim \Lambda} [(R(\pi|s, \lambda, \kappa) \\ & - \tilde{R}(s, \lambda, \kappa)) \nabla_\theta \log p_\theta(\pi|s, \lambda, \kappa)], \end{aligned} \quad (18)$$

where $\tilde{R}(s, \lambda, \kappa)$ is the baseline of expected reward to reduce the variance of the sampled gradients. We use Monte Carlo

Algorithm 1 Customized REINFORCE for UD3RL

Input: Instance distribution \mathcal{S}_I ; radius type distribution \mathcal{S}_λ ; problem size distribution Λ ; number of training epochs E ; number of training instances per epoch \mathbb{D} ; batch size B ; number of solutions n
Output: Trained UD3RL model p_θ

- 1: Initialize policy network parameters θ
- 2: **for** $e \leftarrow 1$ to E **do**
- 3: $D \leftarrow 0$
- 4: **while** $D < \mathbb{D}$ **do**
- 5: $\tilde{B} \leftarrow \min(\mathbb{D} - D, B)$
- 6: $\kappa \sim \text{SAMPLEPROBLEMSIZE}(\Lambda)$
- 7: $\lambda \sim \text{SAMPLERADUSTYPE}(\mathcal{S}_\lambda)$
- 8: $s_b \sim \text{SAMPLEINSTANCE}(\mathcal{S}_I), \forall b \in \{1, \dots, \tilde{B}\}$
- 9: $\pi_b^j \sim \text{SAMPLESOLUTION}(p_\theta(\cdot | s_b, \lambda, \kappa)), \forall j \in \{1, \dots, n\}, \forall b \in \{1, \dots, \tilde{B}\}$
- 10: Compute gradient $\nabla J(\theta)$ according to Eq. (19)
- 11: $\theta \leftarrow \text{ADAM}(\theta, \nabla J(\theta))$
- 12: $D \leftarrow D + \tilde{B}$
- 13: **end while**
- 14: **end for**

sampling to approximate J by training the policy with mini-batches of instances and sampling multiple solutions for each instance. In specific, given B instances $\{s_b\}_{b=1}^B$ with radius type λ and problem size κ and n sampled solutions $\{\pi_b^j\}_{j=1}^n$ for each instance s_b , we calculate the approximate gradient as below,

$$\begin{aligned} \nabla J(\theta) \simeq & \frac{1}{Bn} \sum_{b=1}^B \sum_{j=1}^n (R(\pi_b^j | s_b, \lambda, \kappa) \\ & - \tilde{R}(s_b, \lambda, \kappa)) \nabla_\theta \log p_\theta(\pi_b^j | s_b, \lambda, \kappa), \end{aligned} \quad (19)$$

where we set $\tilde{R}(s_b, \lambda, \kappa) = \frac{1}{n} \sum_{j=1}^n R(\pi_b^j | s_b, \lambda, \kappa)$ and force different second nodes to sample the n tours for each CETSP following [10].

Radius Type and Problem Size Sampling. To strengthen the capability of our UD3RL in solving various CETSPs, we train it with instances of different radius types and multiple sizes at the same time. In specific, we sample a radius type and a problem size from predefined sets \mathcal{S}_λ and Λ respectively for each minibatch and then generate training instances of the corresponding radius type and problem size for optimization as in Eq. (19).

V. EXPERIMENTS

A. Experimental Setup

Problems and Training. We conduct extensive experiments to validate the effectiveness of UD3RL on CETSP across different radius configurations and problem scales. Unlike existing neural heuristics that train separate models for each problem configuration, we train a unified UD3RL model capable of generalizing across varying problem sizes and neighborhood radius types. The training data consists of 100,000 randomly generated instances per epoch, with 2D coordinates uniformly sampled from $[0, 1]^2$. Problem sizes are uniformly drawn from

TABLE I: Results on CETSP instances with different problem sizes and radius types (constant radii: neighborhood radius is fixed; random radii: neighborhood radius is uniformly sampled from a predefined range).

Method	Constant radii n=20			Constant radii n=50			Constant radii n=100			Constant Radii
	Obj.	Gap	Time	Obj.	Gap	Time	Obj.	Gap	Time	Avg. Gap
LKH	2.78	2.58%	37.17s	4.32	2.37%	3.48m	6.65	1.53%	12.15m	2.16%
ORtools	2.92	7.75%	1.67m	4.35	3.08%	3.41m	6.85	4.58%	6.68m	5.14%
PyVRP	2.94	8.49%	36.83s	4.41	4.50%	1.08m	6.71	2.44%	1.95m	5.14%
GA	2.92	7.75%	1.40m	4.45	5.45%	8.07m	7.02	7.18%	17.08m	6.79%
POMO-SOCP	2.78	2.58%	10.66s	4.36	3.32%	17.16s	6.80	3.82%	29.24s	3.24%
POMO-SOCP-Aug	2.73	0.74%	24.89s	4.24	0.47%	48.29s	6.62	1.07%	1.46m	0.76%
UD3RL	2.74	1.11%	0.05s	4.26	0.95%	0.16s	6.62	1.07%	0.87s	1.04%
UD3RL-Aug	2.71	0.00%	0.88s	4.22	0.00%	1.76s	6.55	0.00%	4.35s	0.00%
Method	Random radii n=20			Random radii n=50			Random radii n=100			Random Radii
	Obj.	Gap	Time	Obj.	Gap	Time	Obj.	Gap	Time	Avg. Gap
LKH	3.41	5.25%	38.97s	4.48	2.99%	3.88m	5.68	4.60%	11.80m	4.28%
ORtools	3.29	1.54%	1.67m	4.58	5.29%	3.40m	5.96	9.76%	6.68m	5.53%
PyVRP	3.44	6.17%	37.72s	4.61	5.98%	1.07m	6.03	11.05%	2.12m	7.73%
GA	3.62	11.73%	1.41m	4.68	7.59%	5.75m	6.05	11.42%	12.72m	10.24%
POMO-SOCP	3.38	4.32%	13.18s	4.49	3.22%	20.74s	5.60	3.13%	35.91s	3.56%
POMO-SOCP-Aug	3.26	0.62%	26.63s	4.39	0.92%	49.67s	5.51	1.47%	1.67m	1.00%
UD3RL	3.27	0.93%	0.06s	4.40	1.15%	0.15s	5.50	1.29%	0.85s	1.12%
UD3RL-Aug	3.24	0.00%	0.88s	4.35	0.00%	1.76s	5.43	0.00%	4.33s	0.00%

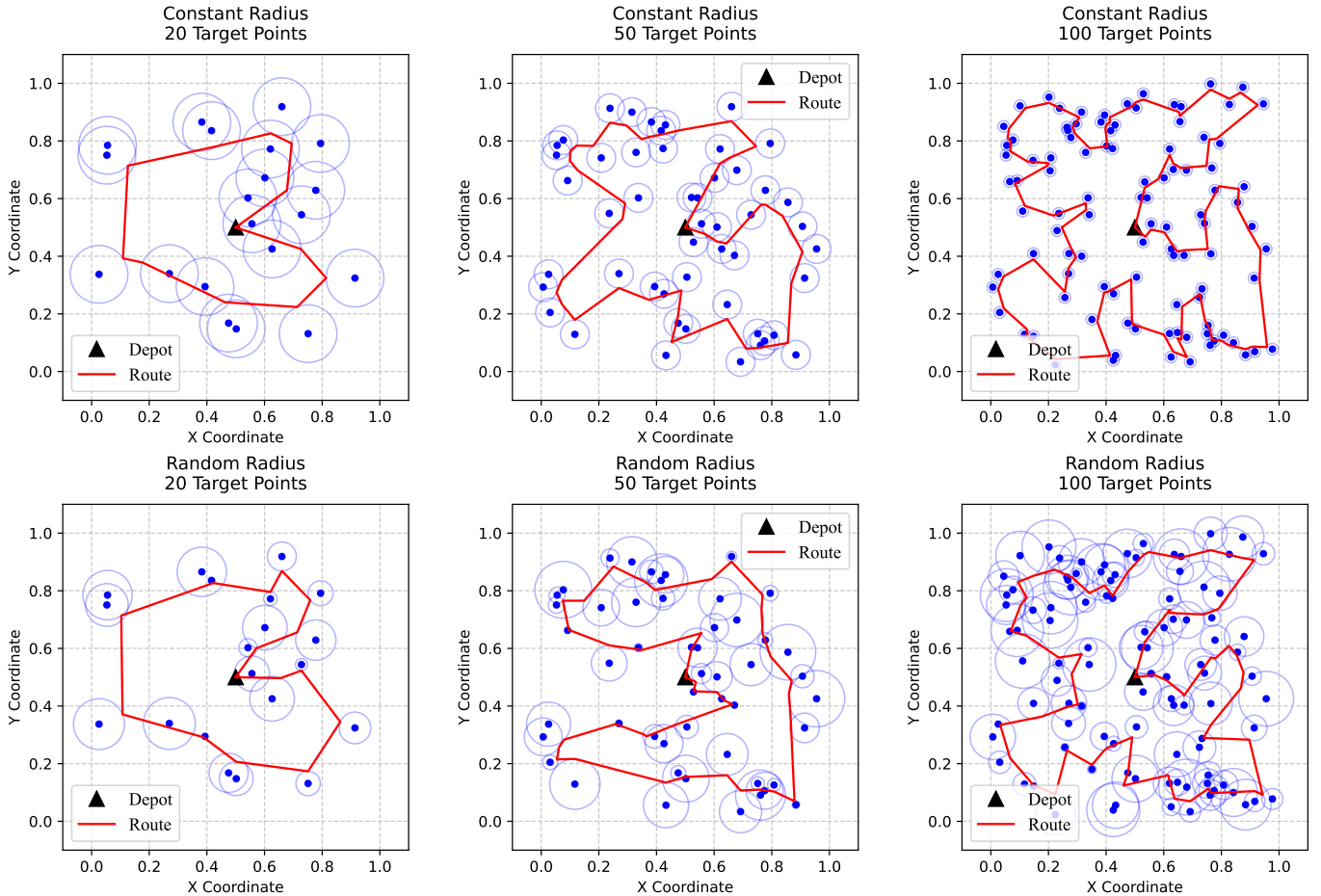


Fig. 4: Visualization of CETSP solutions obtained by UD3RL-Aug across different problem scales. The top row shows results under the constant radius configuration, while the bottom row corresponds to the random radius configuration.

$\Lambda = \{20, 40, 60, 80, 100\}$, representing the number of target nodes in each instance. For radius configurations, two types are considered: (i) constant radii, where $r = 0.1, 0.05, 0.05, 0.01$, and 0.01 for $n = 20, 40, 60, 80$, and 100 , respectively; and (ii) random radii, where each radius is uniformly sampled from $[0, 0.1]$. We train UD3RL for 1000 epochs using the Adam optimizer with learning rate 10^{-4} and weight decay 10^{-6} . The batch size is set to 64. Our network architecture employs a 3-layer Transformer encoder with 8 attention heads and a hidden dimension of 128.

Baselines. We compare UD3RL with a hybrid DRL–SOCP method and four heuristic methods. The hybrid DRL–SOCP method integrates POMO with SOCP (i.e., POMO-SOCP), where POMO determines the node visiting sequence and SOCP computes the precise waypoint within each neighborhood. The heuristic methods include LKH, OR-Tools [36], PyVRP [37], and a genetic algorithm (GA) [5]. In these heuristics, the optimization process first establishes the node visiting sequence and then applies various operators to generate new candidate solutions. SOCP is subsequently used to optimize the specific waypoints within neighborhoods, thereby evaluating the fitness of each solution. The optimization of node sequences and waypoints proceeds iteratively until the maximum number of iterations is reached.

Instance Augmentation. We apply instance augmentation to enhance the inference performance of UD3RL and POMO-SOCP. Following prior work [10], we generate eight transformed instances using rotation and flipping operations that preserve solution optimality due to geometric symmetry, i.e., $(cx', cy') \in \{(cx, cy), (cy, cx), (cx, 1 - cy), (cy, 1 - cx), (1 - cx, cy), (1 - cy, cx), (1 - cx, 1 - cy), (1 - cy, 1 - cx)\}$. Each test instance is solved across all eight augmented versions in parallel, and the best solution is selected. Results obtained with this strategy are denoted with the suffix “-Aug.”

Metrics & Inference. Evaluation is conducted using three metrics: objective value (Obj.), optimality gap (Gap), and runtime (Time). The Obj. represents the average traveling distance within each instance group. The Gap is defined as the percentage difference between a method’s Obj. and the best Obj. achieved across all methods for that group. The Time corresponds to the total runtime required for solving all instances in a group. For each configuration, we generate 100 random test instances under both constant and random radius settings with problem sizes $n \in \{20, 50, 100\}$. To assess generalization, we further evaluate larger scales $n \in \{150, 200, 300, 500\}$ as well as publicly available CETSP benchmark instances¹. All experiments are conducted on an NVIDIA GeForce RTX 4080 Laptop GPU (12 GB) paired with an Intel i9-13980HX CPU. We will make our dataset and implementation code publicly available upon acceptance.

B. Comparison Study

We evaluate all methods on instances with both constant and random radius configurations across three problem scales, $n \in \{20, 50, 100\}$, generating 100 random instances for each setting. The comparison results are summarized in Table I,

where the last column reports the average gap (Avg. Gap) of each method across all scales. For CETSP instances with constant radii, UD3RL achieves superior performance over all baselines, with further improvements when combined with instance augmentation. Results on random radius instances exhibit a similar trend: UD3RL-Aug consistently delivers the best solutions across all cases. Notably, the Avg. The Gap shows that UD3RL’s advantage over conventional heuristics becomes more pronounced under random radius settings. This suggests that the neural network effectively extracts features of the random radii, enabling the DRL agent to learn policies that select appropriate waypoints to minimize tour length. Fig. 4 visualizes example CETSP solutions obtained by UD3RL, illustrating well-optimized routing paths that effectively navigate through node neighborhoods and shorten tour length, thereby confirming UD3RL’s ability to jointly address discrete node selection and continuous waypoint determination.

Beyond solution quality, UD3RL also demonstrates remarkable computational efficiency, solving all test cases in under one second (and under five seconds with instance augmentation), compared to the tens of seconds or even tens of minutes required by traditional heuristics. In particular, the hybrid method POMO-SOCP incurs significantly higher runtimes due to the time-consuming SOCP component. These results highlight UD3RL’s efficiency in solving CETSP problems across different configurations and problem scales.

C. Generalization Study

To evaluate the generalization ability of UD3RL, we conduct three sets of experiments: (1) applying the trained model to larger problem sizes with random radii $n \in \{150, 200, 300, 500\}$; (2) testing on alternative node distributions with random radii, including clustered and mixed uniform–clustered settings; and (3) testing on varying radius ranges, with large radii in $[0.05, 0.15]$ and small radii in $[0.01, 0.05]$. The generated test data for (2) and (3) are illustrated in Fig. 5, where the left plot (“Uniform”) shows an example of the training data with random radii, highlighting the differences between training and test distributions. For each setting, we generate 100 instances, and the corresponding experimental results are summarized in Table II.

For problem size generalization, the results in the upper part of Table II highlight the scalability of UD3RL, which achieves the best solutions with the lowest runtime. In contrast, the hybrid POMO-SOCP method and several conventional heuristics show clear performance degradation as problem size increases. For instance, the gap of POMO-SOCP rises from 2.21% to 15.15%, while GA exceeds 12% for instances with $n = 200$ and $n = 500$. Moreover, UD3RL’s efficiency advantage becomes increasingly pronounced at larger scales, requiring only 42.70 seconds to solve all 500-node instances, compared with hours for conventional approaches.

For node distribution generalization, the results in the lower-left part of Table II indicate that UD3RL consistently achieves the best solutions, demonstrating its robustness across diverse spatial configurations. By comparison, traditional methods such as OR-Tools, PyVRP, and GA yield markedly inferior

¹<https://www.minlp.org/library/problem/index.php?i=65>

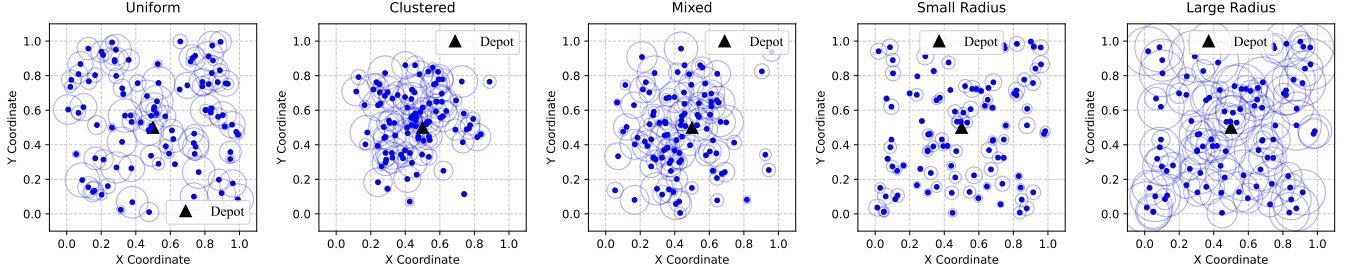


Fig. 5: Visualization of instances with various data distributions and radius ranges.

TABLE II: Generalization results on larger problem sizes, alternate node distributions, and varying radius ranges.

Method	n=150			n=200			n=300			n=500		
	Obj.	Gap	Time	Obj.	Gap	Time	Obj.	Gap	Time	Obj.	Gap	Time
LKH	6.17	4.93%	43.02m	6.78	4.79%	1.15h	7.82	5.25%	2.94h	9.24	3.70%	6.25h
ORtools	6.19	5.27%	6.70m	7.05	8.96%	6.72m	7.93	6.73%	13.45m	10.33	15.94%	13.99m
PyVRP	6.06	3.06%	4.73m	7.11	9.89%	7.10m	7.89	6.19%	41.98m	10.75	20.65%	1.15h
GA	6.09	3.57%	52.44m	7.42	14.68%	1.15h	7.95	7.00%	7.45h	10.05	12.79%	13.35h
POMO-SOCP	6.13	4.25%	47.61s	6.72	3.86%	1.09m	8.05	8.34%	1.45m	10.26	15.15%	2.25m
POMO-SOCP-Aug	6.00	2.04%	1.77m	6.52	0.77%	2.35m	7.62	2.56%	3.37m	10.07	13.02%	7.40m
UD3RL	5.95	1.19%	2.63s	6.55	1.24%	3.37s	7.53	1.39%	15.21s	9.03	1.35%	42.70s
UD3RL-Aug	5.88	0.00%	8.82s	6.47	0.00%	14.54s	7.43	0.00%	30.75s	8.91	0.00%	1.42m
Method	Clustered (n=100)			Mixed (n=100)			Small radii (n=100)			Large radii (n=100)		
	Obj.	Gap	Time	Obj.	Gap	Time	Obj.	Gap	Time	Obj.	Gap	Time
LKH	3.89	2.64%	21.20m	4.84	3.64%	21.30m	6.22	2.47%	18.31m	4.20	4.48%	21.11m
ORtools	4.23	11.61%	6.69m	5.79	23.98%	6.69m	6.97	14.83%	6.69m	5.08	26.37%	5.42m
PyVRP	4.34	14.51%	3.05m	5.26	12.63%	3.05m	6.80	12.03%	2.65m	5.18	28.86%	3.03m
GA	4.25	12.14%	34.62m	5.16	10.49%	33.77m	6.79	11.86%	33.06m	5.17	28.61%	30.30m
POMO-SOCP	4.01	5.80%	33.05s	4.97	6.42%	33.63s	6.35	4.61%	34.21s	4.23	5.22%	33.41s
POMO-SOCP-Aug	3.82	0.79%	1.29m	4.81	3.00%	1.44m	6.14	1.15%	1.45m	4.17	3.73%	1.57m
UD3RL	3.85	1.58%	0.71s	4.74	1.50%	0.71s	6.13	0.99%	0.74s	4.07	1.24%	1.72s
UD3RL-Aug	3.79	0.00%	4.40s	4.67	0.00%	4.31s	6.07	0.00%	4.37s	4.02	0.00%	4.32s

performance, with gaps exceeding 10% relative to the best solutions (i.e., UD3RL-Aug).

For radius range generalization, the results in the lower-right part of Table II show that UD3RL achieves the best solutions with the lowest computation time across all instances, demonstrating its effectiveness in handling diverse neighborhood constraints. Traditional methods, however, exhibit substantial performance fluctuations across different configurations; for example, OR-Tools, PyVRP, and GA incur gaps exceeding 20% on instances with large radii.

D. Benchmark Study

To further verify the effectiveness of UD3RL, we compare it with the baselines on nine benchmark instances. Specifically, six instances are selected under the constant radius configuration, and three instances with the “rdmRad” suffix are selected under the random radius configuration. These benchmark instances provide a rigorous evaluation by comparing against established best-known solutions [8]. Table III displays the results, with the second-best solutions highlighted in bold. According to the results, we observe that UD3RL outperforms all baselines without instance augmentation in all benchmark cases, with gaps generally below 7%. Additionally, UD3RL-Aug achieves even stronger performance, attaining gaps be-

tween 1.36% and 3.91% relative to the best-known solutions. Since the node distributions in the benchmark instances differ considerably from the uniform distribution in training, the experimental results also indicate that UD3RL has a strong out-of-distribution generalization capability.

E. Performance Analysis in Dynamic Scenario

Given UD3RL’s superior computational efficiency, we extend its applicability to dynamic scenarios where rapid solution adaptation is critical. In dynamic CETSP, new requests (dynamic target nodes) appear during tour execution, requiring real-time route adjustments. Our approach leverages the pre-trained UD3RL model to handle such scenarios without additional training. When dynamic nodes appear, the model re-encodes all remaining nodes along with the newly appeared requests, initializes the current state based on the partial tour already executed and current location, and then generates an updated solution. This process is detailed in Algorithm 2.

We evaluate UD3RL against three baseline methods: Cheapest Insertion (CI) [38], [39], widely used in practical industrial scenarios; Modified Regret Insertion (MRI); and Modified Greedy Insertion (MGI) [40] proposed by Meituan, one of China’s largest food delivery platforms. Following [41], we create dynamic scenarios with random radii,

TABLE III: Results on benchmark instances.

Instance	Metrics	Best Known	LKH	ORtools	PyVRP	GA	POMO-SOCP	POMO-SOCP-Aug	UD3RL	UD3RL-Aug
team1_100	Obj. Gap Time	307.34 0.00% -	353.68 15.08% 4.00s	351.14 14.25% 4.01s	357.11 16.19% 2.31s	347.19 12.97% 5.09s	339.28 10.39% 0.50s	319.65 4.01% 0.75s	315.16 2.54% 0.21s	313.30 1.94% 0.49s
team6_500	Obj. Gap Time	225.22 0.00% -	244.96 8.76% 20.04s	249.92 10.97% 26.64s	252.60 12.16% 19.53s	253.94 12.75% 28.07s	312.96 38.96% 2.11s	267.41 18.73% 9.32s	243.71 8.21% 1.31s	229.92 2.09% 7.71s
team1_100rdmRad	Obj. Gap Time	388.54 0.00% -	432.21 11.24% 4.29s	459.52 18.27% 4.01s	451.30 16.15% 2.82s	457.19 17.67% 5.94s	426.08 9.66% 0.61s	397.66 2.35% 1.65s	405.17 4.28% 0.21s	393.81 1.36% 0.62s
team6_500rdmRad	Obj. Gap Time	666.15 0.00% -	739.51 11.01% 77.59s	744.24 11.72% 63.01s	766.82 15.11% 60.79s	739.88 11.07% 42.93s	755.12 13.36% 2.17s	719.85 8.06% 10.89s	708.66 6.38% 1.30s	678.72 1.89% 7.67s
rotatingDiamonds3	Obj. Gap Time	380.88 0.00% -	396.83 4.19% 2.21s	436.10 14.50% 4.02s	439.46 15.38% 4.80s	444.74 16.77% 9.96s	410.33 7.73% 0.73s	396.61 4.13% 1.32s	395.88 3.94% 0.37s	395.76 3.91% 0.45s
bubbles2	Obj. Gap Time	428.28 0.00% -	459.22 7.22% 0.57s	442.53 3.33% 2.04s	450.81 5.26% 1.91s	468.90 9.48% 3.78s	438.23 2.32% 0.46s	436.28 1.87% 0.62s	434.74 1.51% 0.16s	434.74 1.51% 0.14s
bubbles3	Obj. Gap Time	530.73 0.00% -	573.93 8.14% 1.20s	596.42 12.38% 4.01s	561.22 5.74% 3.05s	581.68 9.60% 6.08s	658.53 24.08% 0.61s	560.41 5.59% 0.81s	551.64 3.94% 0.26s	544.38 2.57% 0.28s
chaoSingleDep	Obj. Gap Time	1039.61 0.00% -	1104.10 6.20% 5.46s	1089.39 4.79% 4.01s	1095.78 5.40% 5.42s	1110.37 6.81% 10.41s	1129.25 8.62% 0.75s	1098.67 5.68% 1.54s	1078.71 3.76% 0.42s	1078.71 3.76% 0.61s
pcb442rdmRad	Obj. Gap Time	235.19 0.00% -	262.41 11.57% 57.98s	262.07 11.43% 54.49s	271.69 15.52% 26.20s	267.35 13.67% 29.70s	284.33 20.89% 1.61s	269.12 14.43% 11.42s	252.58 7.39% 1.01s	241.54 2.70% 5.31s

-: Computation times are not provided in the benchmark dataset.

Algorithm 2 Dynamic CETSP Solving using UD3RL

Input: Static nodes $N = \{0, 1, \dots, n\}$ with coordinates and radii; trained UD3RL model p_θ
Output: Complete solution π' visiting all static and dynamic nodes

- 1: Initialize $V_{\text{nodes}} \leftarrow \emptyset$
- 2: Obtain initial solution π_0 and visiting tour $\hat{\tau}$ from the trained UD3RL model
- 3: **for** $t \leftarrow 1$ to $|\pi_0|$ **do**
- 4: Visit waypoint $\hat{\tau}_t$; update V_{nodes}
- 5: **if** dynamic nodes D appear **then**
- 6: Check whether the current partial route covers nodes in D
- 7: **if** any uncovered nodes exist **then**
- 8: Re-encode unvisited static and dynamic nodes N'
- 9: Set current state S_t with the current waypoint
- 10: Update π' and $\hat{\tau}'$ using the trained UD3RL model
- 11: **end if**
- 12: **end if**
- 13: **end for**

including CETSP20-2, CETSP30-4, CETSP50-8, CETSP100-20, CETSP150-30, and CETSP200-50, where the notation CETSP20-2 indicates 20 static nodes with 2 dynamic nodes appearing during execution, and so forth for other configurations, with 100 instances generated for each scenario. The results are shown in Table IV, demonstrating UD3RL's exceptional computational efficiency across all problem scales while maintaining high solution quality, achieving the best

performance in all tested scenarios, and proving its high applicability in dynamic environments.

Fig. 6 visualizes the solutions obtained by our method for the CETSP20-2, CETSP30-4, and CETSP50-8 instances. As shown, UD3RL effectively accommodates dynamic nodes, producing high-quality replanned solutions. This robustness stems from the MDP formulation, which enables the agent to adapt to the current state when dynamic nodes appear, while the efficiency of the UD3RL model supports real-time routing decisions that maintain solution quality. A key observation is that in the replanned routes generated by UD3RL, nodes distant from dynamic requests largely preserve their original visiting sequences and waypoints, whereas those situated nearby adaptively adjust their orders and waypoints, thereby ensuring both solution quality and structural stability of the routes.

F. Ablation Study

To assess the contribution of key components in UD3RL, we conduct ablation studies by (i) removing the k -NN subgraph interaction strategy and (ii) replacing the adapted Transformer encoder with the original version (i.e., post-instance normalizations and standard FF layers), yielding two variants: UD3RL w/o k -NN and UD3RL w/o rev. We evaluate UD3RL and these variants on three problem scales, $n \in \{20, 50, 100\}$, under both constant and random radius configurations. The results, summarized in Table V, show significant performance degradation when either component is removed, with the effect becoming more pronounced on larger instances. These findings confirm the effectiveness of the k -NN subgraph interaction

TABLE IV: Results on dynamic CETSP instances under different problem sizes and newly introduced requests.

Method	CETSP20-2			CETSP30-4			CETSP50-8			CETSP100-20			CETSP150-30			CETSP200-50		
	Obj	Gap	Time	Obj	Gap	Time												
CI	3.10	0.86%	0.06s	3.51	4.96%	0.20s	4.43	4.81%	0.49s	5.95	8.97%	3.66s	7.31	16.85%	10.88s	9.11	24.02%	33.24s
MRI	3.10	0.86%	0.03s	3.50	4.63%	0.10s	4.43	4.81%	0.30s	5.93	8.76%	2.48s	7.25	15.86%	7.74s	9.13	24.35%	29.51s
MGI	3.10	0.86%	0.04s	3.50	4.63%	0.10s	4.43	4.81%	0.30s	5.97	9.45%	2.72s	7.33	17.08%	8.18s	9.00	22.52%	31.14s
UD3RL	3.08	0.00%	0.04s	3.34	0.00%	0.06s	4.23	0.00%	0.10s	5.46	0.00%	0.17s	6.26	0.00%	0.26s	7.34	0.00%	0.35s

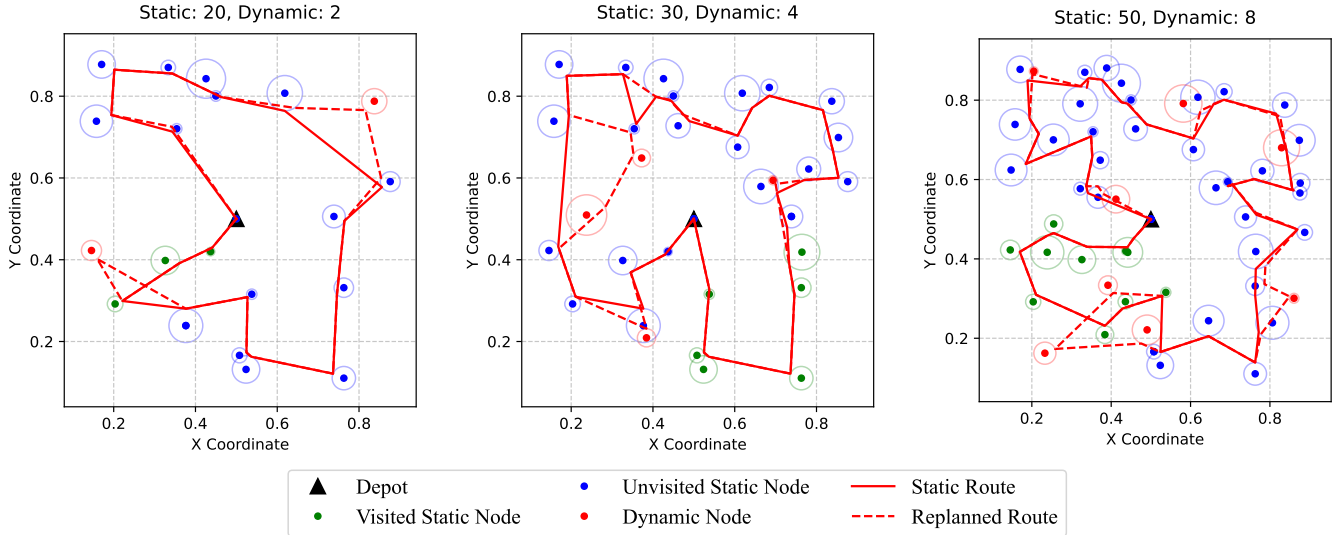


Fig. 6: Visualization of dynamic CETSP solutions across different problem scales and numbers of dynamic requests. The solid red line represents the pre-planned route, while the dashed red line shows the replanned segments adapted in response to newly introduced dynamic nodes.

strategy and the adapted Transformer encoder in the overall architecture. Moreover, incorporating these components does not noticeably increase computational time.

TABLE V: Results of our ablation study.

Instances	Metrics	UD3RL	UD3RL w/o k -NN	UD3RL w/o rev	
Constant Radii	n=20	Obj Gap Time	2.74 0.00% 0.05s	2.77 1.09% 0.04s	2.75 0.36% 0.05s
	n=50	Obj Gap Time	4.26 0.00% 0.16s	4.36 2.35% 0.10s	4.34 1.88% 0.12s
	n=100	Obj Gap Time	6.62 0.00% 0.87s	6.71 1.36% 0.77s	6.80 2.72% 0.74s
Random Radii	n=20	Obj Gap Time	3.27 0.00% 0.06s	3.29 0.61% 0.09s	3.31 1.22% 0.08s
	n=50	Obj Gap Time	4.40 0.00% 0.15s	4.45 1.14% 0.18s	4.49 2.05% 0.16s
	n=100	Obj Gap Time	5.50 0.00% 0.85s	5.57 1.27% 0.78s	5.66 2.91% 0.80s

VI. CONCLUSION

This paper presents UD3RL, a novel unified dual-decoder DRL framework that effectively addresses CETSP. Our approach decomposes the CETSP decision-making process into two sequential stages: node selection through a node-decoder

and waypoint determination within neighborhoods via a loc-decoder. The integration of a k -NN subgraph interaction strategy significantly enhances the waypoint determination phase, while our customized REINFORCE algorithm enables unified training across different problem sizes and radius configurations. Extensive experiments show that UD3RL consistently outperforms both the hybrid method POMO-SOCP and conventional heuristics, achieving higher solution quality while maintaining superior efficiency. Moreover, UD3RL demonstrates strong generalization across different problem scales, node distributions, and radius settings, as well as practical applicability in dynamic scenarios. Future work will focus on extending UD3RL to handle extremely large problem instances (e.g., 10k+ nodes) and exploring cooperative routing of multiple agents in the CETSP.

REFERENCES

- [1] F. Carrabs, C. Cerrone, R. Cerulli, and M. Gaudioso, “A novel discretization scheme for the close enough traveling salesman problem,” *Computers & Operations Research*, vol. 78, pp. 163–171, 2017.
- [2] Z. Lei and J.-K. Hao, “An effective memetic algorithm for the close-enough traveling salesman problem,” *Applied Soft Computing*, vol. 153, p. 111266, 2024.
- [3] D. J. Gulczynski, J. W. Heath, and C. C. Price, “The close enough traveling salesman problem: A discussion of several heuristics,” *Perspectives in Operations Research: Papers in Honor of Saul Gass’ 80 th Birthday*, pp. 271–283, 2006.
- [4] H. Liu, Y. Jin, S. Sun, M. Q. Li, and P. Tsotras, “A hybrid of learning-based and heuristic methods for robot path planning,” in *AIAA SCITECH 2022 Forum*. American Institute of Aeronautics and Astronautics, 2022. [Online]. Available: <https://arc.aiaa.org/doi/abs/10.2514/6.2022-2209>

[5] A. Di Placido, C. Archetti, and C. Cerrone, “A genetic algorithm for the close-enough traveling salesman problem with application to solar panels diagnostic reconnaissance,” *Computers & Operations Research*, vol. 145, p. 105831, 2022.

[6] B. Behdani and J. C. Smith, “An integer-programming-based approach to the close-enough traveling salesman problem,” *INFORMS Journal on Computing*, vol. 26, no. 3, pp. 415–432, 2014.

[7] W. P. Coutinho, R. Q. d. Nascimento, A. A. Pessoa, and A. Subramanian, “A branch-and-bound algorithm for the close-enough traveling salesman problem,” *INFORMS Journal on Computing*, vol. 28, no. 4, pp. 752–765, 2016.

[8] W. K. Mennell, *Heuristics for solving three routing problems: Close-enough traveling salesman problem, close-enough vehicle routing problem, and sequence-dependent team orienteering problem*. University of Maryland, College Park, 2009.

[9] W. Kool, H. Van Hoof, and M. Welling, “Attention, learn to solve routing problems,” in the *6th International Conference on Learning Representations (ICLR)*, 2018.

[10] Y.-D. Kwon, J. Choo, B. Kim, I. Yoon, Y. Gwon, and S. Min, “Pomo: Policy optimization with multiple optima for reinforcement learning,” *Advances in Neural Information Processing Systems*, vol. 33, pp. 21 188–21 198, 2020.

[11] W. Mennell, B. Golden, and E. Wasil, “A steiner-zone heuristic for solving the close-enough traveling salesman problem,” in *2th INFORMS computing society conference: operations research, computing, and homeland defense*, 2011.

[12] X. Wang, B. Golden, and E. Wasil, “A steiner zone variable neighborhood search heuristic for the close-enough traveling salesman problem,” *Computers & Operations Research*, vol. 101, pp. 200–219, 2019.

[13] F. Carrabs, C. Cerrone, R. Cerulli, and C. D’Ambrosio, “Improved upper and lower bounds for the close enough traveling salesman problem,” in *Green, Pervasive, and Cloud Computing: 12th International Conference, GPC 2017, Cetara, Italy, May 11–14, 2017, Proceedings 12*. Springer, 2017, pp. 165–177.

[14] F. Carrabs, C. Cerrone, R. Cerulli, and B. Golden, “An adaptive heuristic approach to compute upper and lower bounds for the close-enough traveling salesman problem,” *INFORMS Journal on Computing*, vol. 32, no. 4, pp. 1030–1048, 2020.

[15] H. Guo, Q. Peng, Z. Cao, and Y. Jin, “Drl-searcher: A unified approach to multirobot efficient search for a moving target,” *IEEE Transactions on Neural Networks and Learning Systems*, vol. 35, no. 3, pp. 3215–3228, 2024.

[16] X. Chen and Y. Tian, “Learning to perform local rewriting for combinatorial optimization,” in *Advances in Neural Information Processing Systems*, vol. 32, 2019, pp. 6281–6292.

[17] A. Hottung and K. Tierney, “Neural large neighborhood search for the capacitated vehicle routing problem,” *arXiv preprint arXiv:1911.09539*, 2019.

[18] Y. Wu, W. Song, Z. Cao, J. Zhang, and A. Lim, “Learning improvement heuristics for solving routing problems,” *IEEE Transactions on Neural Networks and Learning Systems*, 2021.

[19] P. R. d O Costa, J. Rhuggenaath, Y. Zhang, and A. Akcay, “Learning 2-opt heuristics for the traveling salesman problem via deep reinforcement learning,” in *Asian Conference on Machine Learning*. PMLR, 2020, pp. 465–480.

[20] M. Kim, J. Park *et al.*, “Learning collaborative policies to solve np-hard routing problems,” in *Advances in Neural Information Processing Systems*, vol. 34, 2021, pp. 10 418–10 430.

[21] Y. Ma, J. Li, Z. Cao, W. Song, L. Zhang, Z. Chen, and J. Tang, “Learning to iteratively solve routing problems with dual-aspect collaborative transformer,” in *Advances in Neural Information Processing Systems*, vol. 34, 2021, pp. 11 096–11 107.

[22] I. Bello, H. Pham, Q. V. Le, M. Norouzi, and S. Bengio, “Neural combinatorial optimization with reinforcement learning,” in *International Conference on Learning Representations(Workshop)*, 2017.

[23] M. Nazari, A. Oroojlooy, L. Snyder, and M. Takáć, “Reinforcement learning for solving the vehicle routing problem,” in *Advances in Neural Information Processing Systems*, vol. 31, 2018, pp. 9839–9849.

[24] L. Xin, W. Song, Z. Cao, and J. Zhang, “Multi-decoder attention model with embedding glimpse for solving vehicle routing problems,” in *Proceedings of the AAAI Conference on Artificial Intelligence*, vol. 35, no. 13, 2021, pp. 12 042–12 049.

[25] M. Kim, J. Park, and J. Park, “Sym-nco: Leveraging symmetry for neural combinatorial optimization,” in *Advances in Neural Information Processing Systems*, 2022.

[26] B. Li, G. Wu, Y. He, M. Fan, and W. Pedrycz, “An overview and experimental study of learning-based optimization algorithms for the vehicle routing problem,” *IEEE/CAA Journal of Automatica Sinica*, vol. 9, no. 7, pp. 1115–1138, 2022.

[27] F. Berto, C. Hua, J. Park, L. Luttmann, Y. Ma, F. Bu, J. Wang, H. Ye, M. Kim, S. Choi *et al.*, “Rl4co: an extensive reinforcement learning for combinatorial optimization benchmark,” in *Proceedings of the 31st ACM SIGKDD Conference on Knowledge Discovery and Data Mining* V. 2, 2025, pp. 5278–5289.

[28] O. Vinyals, M. Fortunato, and N. Jaitly, “Pointer networks,” in *Advances in Neural Information Processing Systems*, vol. 28, 2015, pp. 2692–2700.

[29] A. Vaswani, N. Shazeer, N. Parmar, J. Uszkoreit, L. Jones, A. N. Gomez, Ł. Kaiser, and I. Polosukhin, “Attention is all you need,” in *Advances in Neural Information Processing Systems*, vol. 30, 2017.

[30] F. Luo, X. Lin, F. Liu, Q. Zhang, and Z. Wang, “Neural combinatorial optimization with heavy decoder: Toward large scale generalization,” *Advances in Neural Information Processing Systems*, vol. 36, pp. 8845–8864, 2023.

[31] Y. Li, J. Guo, R. Wang, and J. Yan, “T2t: From distribution learning in training to gradient search in testing for combinatorial optimization,” *Advances in Neural Information Processing Systems*, vol. 36, pp. 50 020–50 040, 2023.

[32] F. Berto, C. Hua, N. G. Zepeda, A. Hottung, N. Wouda, L. Lan, K. Tierney, and J. Park, “RouteFinder: Towards foundation models for vehicle routing problems,” in *ICML 2024 Workshop on Foundation Models in the Wild (Oral)*, 2024, <https://github.com/ai4co/routefinder>. [Online]. Available: <https://openreview.net/forum?id=hCiaiZ6e4G>

[33] N. Shazeer, “Glu variants improve transformer,” *arXiv preprint arXiv:2002.05202*, 2020.

[34] B. Zhang and R. Sennrich, “Root mean square layer normalization,” *Advances in Neural Information Processing Systems*, vol. 32, 2019.

[35] R. J. Williams, “Simple statistical gradient-following algorithms for connectionist reinforcement learning,” *Machine Learning*, vol. 8, no. 3, pp. 229–256, 1992.

[36] V. Furnon and L. Perron, “Or-tools routing library,” Google. [Online]. Available: <https://developers.google.com/optimization/routing/>

[37] N. A. Wouda, L. Lan, and W. Kool, “Pyvrp: A high-performance vrp solver package,” *INFORMS Journal on Computing*, 2024.

[38] X. Wang, L. Wang, S. Wang, J.-f. Chen, and C. Wu, “An xgboost-enhanced fast constructive algorithm for food delivery route planning problem,” *Computers & Industrial Engineering*, vol. 152, p. 107029, 2021.

[39] X. Li, W. Luo, M. Yuan, J. Wang, J. Lu, J. Wang, J. Lü, and J. Zeng, “Learning to optimize industry-scale dynamic pickup and delivery problems,” in *2021 IEEE 37th international conference on data engineering (ICDE)*. IEEE, 2021, pp. 2511–2522.

[40] Q. Zhou, H. Zheng, S. Wang, J. Hao, R. He, Z. Sun, X. Wang, and L. Wang, “Two fast heuristics for online order dispatching,” in *2020 IEEE Congress on Evolutionary Computation (CEC)*. IEEE, 2020, pp. 1–8.

[41] Z. Zhang, J. Yang, Z. Cao, and H. C. Lau, “Neuro-ins: A learning-based one-shot node insertion for dynamic routing problems,” *IEEE Transactions on Knowledge and Data Engineering*, 2025.